Ibn Al-Haitham Journal for Pure and Applied Science | مجلة إبن الهيثم للعلوم الصرفة و التطبيقية
No. 2 Vol. 25 Year 2012 | 2012 السنة 25 المجلد 2 العدد

Study the Effect of Fuel Pressure on the Operating and Phases Parameters For PF400J Dense Plasma Focus Device

R. H. Majeed, M. K. Jassim, F. M. Hady
Department of Physics, College of Education Ibn Al-Haitham, University of Baghda
Received in:19 February 2012, Accepted in: 17 June 2012

Abstract

Theoretical calculations are achieved to study the effect of different deuterium pressures on various characteristics parameters for PF400J plasma focus using an international computer code. Axial and radial velocities, voltage tube, plasma temperatures, and neutron yields at different operating deuterium pressures are computed. Neutron emission has been calculated in the device. The maximum total neutron yield calculated is of the order of (10^5) and (10^6) neutrons per shot for entire pressure used. The computed results agree reasonably well with the published neutron yield curves.
Keywords: plasma focus, neutron yield, deuterium gas, Lee code

Introduction

The device which can generate, accelerate and pinch plasma by electromagnetic forces is called dense plasma focus (DPF). The DPF was invented in 1960s and is used in many types of research [1]. In this device the plasma is pinched in very short time (ns), however it is hot and dense enough to enhance nuclear fusion reactions, making the DPF to be multi – radiation source. The DPF works in pulsed mode because the discharge lasts few tens of (μs), hence the DPF efficiently operated in a repetitive regime. Mainly there are two types of DPF, Mather and Filippov configurations. And basically they differ in the geometric design, where the former is adjusted vertically while the latter is adjusted horizontal. Further they differ in the dimension of inner and outer electrodes which affect the direction of motion of the accelerated plasma.

The plasma focus is divided into two sections. The first is a pre – pinch (axial) section. The function of this section is primarily to delay the pinch until the capacitor discharge approaches its maximum current. This is done by driving a current sheet down an axial (acceleration) section until the capacitor current approaches its peak. Then the current sheet is allowed to undergo transition into a radial compression phase. Thus the pinch starts and occurs at the top of the current pulse [2].

Several models were developed to simulate the plasma motion in both the axial and the radial phases [3 – 6]. One of the most interesting models was developed by Lee [3]. He developed the model with a complete description of the plasma focus dynamics in the axial and in the radial phases. Although in the literature the DPF is divided into three phases, the code divides the DPF into five phases: Axial acceleration Phase, Radial Inward Shock Phase, Radial Reflected Shock Phase, Pinch Phase, and Expanded Column Phase. To calculate several parameters on DPF based on many model and mechanism Lee continually updating the code [3]. The description [7], theory [8], code [3] and a broad range of results of the model are available for download from the "Universal Plasma Laboratory Facility" website.

In addition, the mechanics of fitting the model to a measured current trace which is described in the Internet Course notes is also available [2].

We configure the Lee model code (version RADPFV5.15de.xls) which is executed in Microsoft Excel Visual Basic that is converted from original old version written in GWBASIC. We choose a PF400J machine device to execute in our simulation. The PF400J machine is small and fast plasma focus operating in deuterium. We start with the following published bank and tube parameters of this device [9]:

The system operates at low energy in the hundred of joules range ($880\ \mathrm{nF}$ capacitor bank, $38\ \mathrm{nH}$, $20-35\ \mathrm{kV}$, $176-539\ \mathrm{J}$, $\sim 300\ \mathrm{ns}$ current rise time). We follow fitting procedure in the same manner as given in paper [10] to achieve the numerical experiment. We use Bank parameters: the static inductance $L_0 = 40\ \mathrm{nH}$, the storage capacitance $C_0 = 0.95\ \mu\mathrm{F}$, and stray circuit resistance $r_0 = 10\ \mathrm{m\Omega}$. Tube parameters: the tube outer radius $r_b = 1.55\ \mathrm{cm}$, the inner radius $r_a = 0.6\ \mathrm{cm}$, and the anode length $z_0 = 1.7\ \mathrm{cm}$. Operational parameters: are operating voltage $V_0 = 28\ \mathrm{kV}$ and operating initial pressure of deuterium gas $P_0 = \cdots\ \mathrm{Torr}$. The computed total current waveform is fitted to the measured waveform by putting model parameters: the axial mass swept – up factor $f_m = 0.08$, the tube current flow factor $f_c = 0.7$, the radial mass swept – up factor $f_{mr} = 0.11$ and the radial current factor $f_{cr} = 0.7$ so that the computed waveform matches with the measured published waveform [9] (Fig. 1).

Once the fitting is done such that the two traces practically inseparable the other computed properties including axial and radial phase dynamics, energy distributions and radiation are all realistic. The current trace of the focus is one of the best indicators of gross performance such that the information is rapidly apparent from the current trace [2]. Numerical experiments are then carried out at an operating voltage of $(28\ \mathrm{kV})$ and at various initial deuterium fuel pressures.

The numerical simulations give insights on factors that affect the dynamic of plasma focus devices by illustrating them graphically. However, the code is executed for certain operating pressure at once. Hence collecting data for various fuel pressures of working gas yield a comparative database of how the dynamic of plasma and characteristics of the device change. We look for the effect of pressure varying on dynamics factors in both axial, radial phases and neutron yield of PF400J machine.

Theoretical approach

A brief review to the important equations used in the calculations of the different parameters that describing the completely physical behavior for three important phases occurred in machine are given in the international computer code named Lee [10], these phases are explained in the following sections.

Axial Phase

This is described by a snowplow model with an equation of motion:

$$\frac{d^2z}{dt^2} = \left[\frac{f_c^2}{f_m}\frac{\mu_0(\ln c)}{4\pi\rho_0(c^2-1)}\left(\frac{I}{r_a}\right)^2 - \left(\frac{dz}{dt}\right)^2\right]Iz$$

In which z is axial position of the current sheath (m), f_m is fraction of mass swept down the axial direction, f_c is fraction of current flowing in the piston, $c = r_b/r_a$, ρ is gas density, and μ_0 is permeability of free space.

In addition, the electrical characteristics of the circuit have the following parameters:

Where V_0 is initial charge applied to the capacitor, L_0 is circuit stray inductance (H), C_0 is energy storage capacitance (F), and r_0 is stray circuit resistance (ohm).

We also define:

$Z_0 = L_0/C_0$ (Surge impedance, ohm)

$t_0 = (L_0C_0)^{1/2}$ (Note: $2\pi(L_0C_0)^{1/2}$ is the L-C circuit cycle time)
$I_0 = V_0/Z_0$

This is normalized with $\tau = t/t_0$, $\xi = z/z_0$ and $i = I/I_0$, and we have

$$\frac{d^2\xi}{d\tau^2} = \frac{\left[\alpha^2\tau^2 - \left(\frac{d\xi}{d\tau}\right)^2\right]}{\xi},$$

where

$$\alpha^2 = \frac{t_0^2}{\left[\frac{z^2}{(1/a)^2}\frac{f_m}{f_c^2}\frac{4\pi(c^2-1)}{\mu(\ln c)}\right]}$$

f_m is fraction of mass swept down the tube in the axial direction, and f_c is fraction of current flowing in piston.

It incorporates axial phase model parameters: mass and current factors f_m and f_c, and is coupled to a circuit equation:

$$\frac{dI}{dt} = \left[V_0 - \frac{\int I dt}{C_0} - r_0 r - I f_c \frac{\mu}{2\pi}(\ln c)\frac{dz}{dt}\right] I\left[L_0 + \frac{f_c\mu}{2\pi}(\ln c)z\right]$$

Similarly, after normalization, we have:

$$\frac{di}{d\tau} = \left(1 - \int i d\tau - \beta i\frac{d\xi}{d\tau} - \delta i\right)/(1+\beta\xi),$$

where

$\beta = \frac{L_a}{L_0}$ with $L_a = \frac{f_c\mu}{2\pi}(\ln c)z_0$

The normalized equations may be integrated numerically by incrementing τ by an interval, say 0.001, until ξ reaches 1 (ξ is the axial distance of current sheath normalized to the electrode length).

Radial Inward Shock Phase

This phase is described by 4 coupled equations using an elongating slug model. The first equation computes the radial inward shock speed from the driving magnetic pressure.

$$\frac{dr_s}{dt} = -\left[\frac{\mu(\gamma+1)}{\rho_0}\right]^{1/2} \frac{f_c}{\sqrt{f_{mr}}} \frac{1}{4\pi r_p}$$

Where r_p is radial piston position, r_s is radial shock front position, f_{mr} is modified fm value in the radial phase, γ is specific heat ratio of the operating gas, and ρ_0 is the gas density.

This may be normalized with $\kappa_s = r_s/a$, $\kappa_p = r_p/a$, and $\xi_f = z_f/a$ giving:

$\frac{d\kappa_s}{d\tau} = -\alpha\alpha_i \iota/\kappa_p$ Where

$$\alpha_1 = \sqrt{\frac{(\gamma+1)(c^2-1)}{4(\ln c)}} \frac{z_0}{a}\left[\left(\frac{f_m}{f_{mr}}\right)^{1/2}\right]$$

The second equation computes the axial elongation speed of the column.

$$\frac{dz_f}{dt} = -\left(\frac{2}{\gamma+1}\right)\frac{dr_s}{dt}$$

Similarly, this can be normalized to:

$$\frac{d\xi_f}{dt} = -\left(\frac{2}{\gamma+1}\right)\frac{d\kappa_s}{d\tau}$$

The third equation computes the speed of the current sheath, also called the magnetic piston, allowing the current sheath to separate from the shock front by applying an adiabatic approximation.

$$\frac{dr_p}{dt} = \frac{\frac{2}{\gamma+1}\frac{r_s}{r_p}\frac{dr_s}{dt} - \frac{r_p}{\gamma I}\left(1-\frac{r_s^2}{r_p^2}\right)\frac{dI}{dt} - \frac{r_p}{z_f}\left(1-\frac{r_s^2}{r_p^2}\right)\frac{dz_f}{dt}}{\frac{\gamma-1}{\gamma}+\frac{1}{\gamma}\frac{r_s^2}{r_p^2}}$$

r_p is radial piston position, r_s is radial shock front position, and z_f is axial piston position. After normalization, this becomes:

$$\frac{d\kappa_p}{dt} = \frac{\frac{2}{\gamma+1}\frac{\kappa_s}{\kappa_p}\frac{d\kappa_s}{dt} - \frac{\kappa_p}{\gamma\iota}\left(1-\frac{\kappa_s^2}{\kappa_p^2}\right)\frac{d\iota}{dt} - \frac{1}{\gamma+1}\frac{\kappa_p}{\xi_f}\left(1-\frac{\kappa_s^2}{\kappa_p^2}\right)\frac{d\xi_f}{dt}}{\frac{\gamma-1}{\gamma}+\frac{1}{\gamma}\frac{\kappa_s^2}{\kappa_p^2}}$$

The fourth is the circuit equation:

$$\frac{dI}{dt} = \frac{V_0 - \frac{\int I dt}{C_0} - r_0 I - f_c\frac{\mu}{2\pi}\left(\ln\frac{b}{r_p}\right)I\frac{dz_f}{dt} + f_c\frac{\mu}{2\pi}\left(\frac{z_f}{r_p}\right)I\frac{dr_p}{dt}}{L_0 + f_c\frac{\mu}{2\pi}(\ln c)z_0 + f_c\frac{\mu}{2\pi}\left(\ln\frac{b}{r_p}\right)z_f}$$

The normalized form is:

$$\frac{d\iota}{dt}=\frac{1-\int \iota dt+\beta\left(\ln\frac{\kappa_p}{c}\right)\iota\frac{d\xi_f}{d\tau}+\beta\xi_f\iota\frac{d\kappa_p}{d\tau}-\delta\iota}{\left\{1+\beta-\beta_1\left(\ln\frac{\kappa_p}{c}\right)\xi_f\right\}}$$

The model parameters, radial phase mass and current factors, f_{mr} and f_{cr}, are incorporated in the radial phases. Thermodynamic effects due to ionization and excitation are incorporated into these equations, these effects being important for gases other than hydrogen and deuterium. The average temperature and number densities are computed during this phase.
The four equations can then be integrated by applying a time difference, D, as follows:

$\kappa_s=\kappa_s+\frac{d\kappa_s}{d\tau}D$, $\xi_s=\xi_s+\frac{d\xi_f}{d\tau}D$, $\kappa_p=\kappa_p+\frac{d\kappa_p}{d\tau}D$, $\iota=\iota+\frac{d\iota}{d\tau}D$, and $\int \iota d\tau=\int \iota d\tau+\iota D$

The normalized voltage, $v(=V/V_0)$ can be calculated from considering only the inductive component $=d(LI)/dt$, where $L=(\mu/2\pi)(\ln c)z_0+(\mu/2\pi)(\ln b/r_b)z_f$.

The normalized voltage is then:

$$v=\left[\beta-\beta_1\left(\ln\frac{\kappa_p}{c}\right)\xi_f\right]\frac{d\iota}{d\tau}-\beta_1\iota\left[\frac{\xi_f}{\kappa_p}\frac{d\kappa_p}{d\tau}+\left(\ln\frac{d\kappa_p}{c}\right)\frac{d\xi_f}{d\tau}\right]$$

In addition, a communication delay between shock front and current sheath due to the finite small disturbance speed is incorporated by calculating an appropriate delay when integrating the shock speed.

Radial Reflected Shock (RS) Phase

When the shock front hits the axis, because the focus plasma is collision, a reflected shock develops which moves radially outwards, whilst the radial current sheath piston continues to move inwards. Four coupled equations are also used to describe this phase, these being for the reflected shock moving radially outwards, the piston moving radially inwards, the elongation of the annular column and the circuit equation. The same model parameters f_{mr} and f_{cr} are used as in the previous radial phase. The reflected shock is estimated to be $1/3$ of the inward radial shock speed.

$$\frac{dr_r}{dt}=-0.33\left(\frac{dr_s}{dt}\right)_{on\,axis}$$

The equations used are:

a. Piston radial speed

$$\frac{dr_p}{dt}=\frac{-\frac{r_p}{\gamma I}\left(1-\frac{r_s^2}{r_p^2}\right)\frac{dI}{dt}-\frac{r_p}{z_f}\left(1-\frac{r_s^2}{r_p^2}\right)\frac{dz_f}{dt}}{\frac{\gamma-1}{\gamma}+\frac{1}{\gamma}\frac{r_s^2}{r_p^2}}$$

b. Pinch elongation speed

$$\frac{dz_f}{dt}=-\left(\frac{2}{\gamma+1}\right)\left(\frac{dr_s}{dt}\right)_{on\,axis}$$

c. Circuit Equation

$$\frac{dI}{dt}=\frac{V_0-\frac{\int Idt}{C_0}-r_0I-f_c\frac{\mu}{2\pi}\left(\ln\frac{b}{r_p}\right)I\frac{dz_f}{dt}+f_c\frac{\mu}{2\pi}\left(\frac{z_f}{r_p}\right)I\frac{dr_p}{dt}}{L_0+f_c\frac{\mu}{2\pi}(\ln c)z_0+f_c\frac{\mu}{2\pi}\left(\ln\frac{b}{r_p}\right)z_f}$$

d: Pinch voltage

$$V=\frac{\mu}{2\pi}\left[(\ln c)z_0+\left(\ln\frac{b}{r_p}\right)z_f\right]f_c\frac{dI}{dt}+\frac{\mu}{2\pi}\left[\left(\ln\frac{b}{r_p}\right)\frac{dz_f}{dt}+\frac{z_f}{r_p}\frac{dr_p}{dt}\right]f_cI$$

Pinch Phase

Three coupled equations describe this phase; these being the piston radial motion equation, the pinch column elongation equation and the circuit equation, incorporating the same model parameters as in the previous two phases. Thermodynamic effects are incorporated into this phase. When the out-going reflected shock hits the in-going piston the compression enters into the radiative phase in which for gases such as neon, radiation emission may actually enhance the compression where we have included energy loss/gain terms from Joule heating and radiation losses into the piston equation of motion.

The duration of this slow compression phase is set as the time of transit of small disturbances across the pinched plasma column. The computation of this phase is terminated at the end of this duration. The equations used are:

a. Radial speed

$$\frac{dr_p}{dt}=\frac{-\frac{r_p}{\gamma I}\frac{dI}{dt}-\frac{1}{\gamma+1}\frac{r_p}{z_f}\frac{dz_f}{dt}-\frac{4\pi(\gamma-1)}{\mu\gamma z_f}\frac{r_p}{f_cI^1}\frac{dQ}{dt}}{\frac{\gamma-1}{\gamma}}$$

b. Column elongation

$$\frac{dz_f}{dt}=\left[\frac{\mu}{4\pi^2(\gamma+1)\rho_0}\right]^{1/2}\frac{If_c}{r_p}$$

c. Circuit equation

$$\frac{dI}{dt}=\frac{V_0-\frac{\int Idt}{C_0}-\frac{\mu}{2\pi}\left(\ln\frac{b}{r_p}\right)\frac{dz_f}{dt}If_c+\frac{\mu}{2\pi}\frac{z_f}{r_p}\frac{dr_p}{dt}If_c-I(Rf_c+r_0)}{L_0+\frac{\mu}{2\pi}f_c\left[(\ln c)z_0+\ln\frac{b}{r_b}\right]z_f}$$

d. Voltage

$$V=\frac{\mu f_c}{2\pi}I\left[\left(\ln\frac{b}{r_p}\right)\frac{dz_f}{dt}-\frac{z_f}{r_p}\frac{dr_p}{dt}\right]+\frac{\mu f_c}{2\pi}\left[(\ln c)z_0+\left(\ln\frac{b}{r_p}\right)z_f\right]\frac{dI}{dt}+RI$$

In addition, the radiation energies are calculated as follows:

Expanded Column Phase

In this final phase the snow plow model is used, and two coupled equations are used similar to the axial phase. This phase is not considered important as it occurs after the focus pinch. The normalized equations for the circuit and the motion are as follows.

a. Circuit equation:

$$\frac{di}{d\tau} = \frac{1-\int i\,d\tau+\beta i\frac{d\xi_f}{d\tau}e-\delta i}{1+\beta-\beta(\xi-1)e} \quad \text{where} \quad e=(\ln c+1/z)/\ln c$$

b. Motion equation:

$$\frac{d^2\xi}{d\tau^2} = \frac{\left[\alpha^2 i^2 e_1-h^2\left(\frac{d\xi}{d\tau}\right)^2\right]}{1+h^2(\xi-1)} \quad \text{where} \quad e_1=(\ln c+1/4)/\ln c$$

Calculations and Results

Initially we look at variation of tube current with fuel pressure; running PF400J from short – circuit (very high pressure) to a low pressure. To simulate a short circuit we apply very high pressure shot that stops the entire current sheath motion. This shot is just to obtain unloaded case current waveform for comparison with the focusing waveforms at different lower pressures. Figure (2) shows the variation of tube current vs. time for this shot. At this extreme high pressure (100000 Torr) the current waveform is sinusoid ally damped. In real experiment, this shot to ensure that the current sheet moves past the probe before current move fairly slowly so that the current waveform is near sinusoidal [12].

At lower pressure, the variation of current and other properties with pressure are compiled together in the code. The current waveform distorts from damped sinusoid when plasma focus loaded because of the electro – dynamical effects of the plasma motion, including the axial and radial phase dynamics.

Figure (3) illustrates this distortion of current waveform (upper bold curves) for several values of deuterium fuel pressure. The flattening of the current waveform at pressure (11.3 Torr) is evident, however, the current peak is lower and comes earlier than (100000 Torr). The characteristic of current waveform as the pressure lowered is such that the current peak comes earlier and the current trace is continually compressed more. The current waveform, due to the decreased axial phase, has a dip started at (0.32 μs) for a pressure (8.3 Torr), (0.301 μs) for a pressure (5.3 Torr) and (0.178 μs) for a pressure (0.8 Torr). Figure (3) also shows the variation of computed total tube voltage (lower thin curves) during radial phase vs. time. It is clear that increasing pressure leads to lower voltage peak waveform. The start of voltage waveform peak is the end of axial phase and a start of radial pinch phase. Obviously, the tube voltage waveform peaks, which is induced by the rapid plasma motion, coincide with the dip of current. However, in this type of numerical simulation it is hard enough to compare measured and computed tube voltage in term of peak value since the response time of dividers is so poor. Comprehensibility, low pressure case has too fast a voltage drop from peak voltage due to the instantaneously moving radial phase into the expanded column phase. And as mentioned earlier as the pressure increases the current waveform is flattened and it is from the figure that the voltage waveform has very low peak.

Figure (4) shows the variation of axial position and speed vs. time for different gas pressures. Obviously, the axial phase positions (lower thin curves) are decreased as the pressure decreases. The higher pressure results in the plasma last higher time in the axial position before the cut off. At lower pressure, the axial position continues rising at earlier time and longer duration than that of the higher pressure at late time. Since the same curves of axial positions of the plasma for various pressures have different durations in the earlier time, the axial speeds (upper bold curves) in turn have distinguished curves displaying axial phase dynamics in term of speed. As the pressure is increased the axial speed decreased. It shows that the current sheath reaches the end of the axial phase at less than $(0.20\ \mu s)$ with a peak speed of less than $(25\ cm/\mu s)$ for lower pressure used so that the computed current dip comes much too early in (Fig. 3). Thus it is reasonable to correlate the current dip with the radial phase, so the shift of the current dip comes earlier at lower and lower pressures is consistent with higher axial speeds. The current trace is compressed more and more due to the increased axial speed. The current waveform continues to rise and then due to the radial phase dynamics it is forced down to form a dip. At the end of current dip the pinch phase occurs. The expanded Colum phase starts after the end of pinch phase. Now, throughout the entire range of pressures the decreasing axial speed decreases the circuit loading and so the peak current comes late. The high speed would also lower the peak current. The current sheet is accelerated, rapidly reaching nearly its peak speed, and continues accelerating slightly toward its peak speed at the end of the axial phase. Thus for most of its axial position the current sheet is traveling at a speed close to the end – axial speed. Fig (3) also shows that the current sheaths reach the end of the axial phase at $(0.683\ \mu s)$ with a peak speed of $(24.2\ cm/\mu s)$ for pressure $(0.8\ Torr)$ and $(7.09\ cm/\mu s)$ for pressure $11.3\ Torr$. In deuterium the end of axial speed for pressure less than $(5.3\ Torr)$ is observed to be about $(10\ cm/\mu s)$ [13].

Figure (5) displays the tube voltage variation vs. time from start of radial phase for different gas pressures. As pressure decreases the curves are at higher voltage and last shorter time, also the tube voltage peaks are thinner. At pressure $(4.5\ Torr)$ the radial voltage is $(20.9\ kV)$ while it is $(13.9\ kV)$ for a pressure $(8.3\ Torr)$.

Figure (6) displays the variation of plasma temperature peaks at middle of pinch duration vs. time for different gas pressures. The figure shows that plasma temperature has a maximum value and an averaged uniform value. Increasing gas pressure leads to decrease plasma temperature. The plasma temperature peak is $(3.75 \times 10^{7}\ ^{0}K)$ for a pressure $(0.8\ Torr)$ and it is $(1.73 \times 10^{7}\ ^{0}K)$ for a pressure $(2.3\ Torr)$.

Figure (7) shows the variation of radial inward (thin curves) and reflected shock position (bold curves) vs. time for different pressures. The inward shock trajectory curve is decreased from same point $(6\ mm)$ to $(0\ mm)$ for entire pressures value used; however, lower gas pressure suffers shorter duration than higher pressure. Its duration is $(11.1\ \mu s)$ for a pressure $(0.8\ Torr)$ and it is $(36.3\ \mu s)$ for a pressure $(11.3\ Torr)$. When the shock front hits the axis, because the focus plasma is collisional, a reflected shock (linearly increased bold lines) develops and moves radially outwards. We note that the radial trajectories and speeds are difficult to measure, thus the computed radial trajectories and speeds yield insight of how these parameters behave in radial phase.

Figure (8) shows the variation of radial piston (current sheath) vs. time for various pressures. As time progresses the radial piston sharply falls down reaching to time point such that it linearly decreased. In spite of that, the shock front hits the axis (Figure 7); the radial

current sheath piston continues to move inwards. The piston continues to compress inwards until it hits the out – going reflected shock front. The point where the piston meets the reflected shock is the point of maximum compression, which labels as radial position r_{min}. The r_{min} has value of $0.08\ cm$ for pressure less than $(5.3\ Torr)$ and $(0.09\ cm)$ for this pressure and higher.

Figure (9) shows the variation of radial pinch elongation speed vs. time for different gas pressures. It is clear that the radial pinch elongation has the similar behavior except that it has longer duration as the pressure increased. It has peak at $(8.46\ mm)$ for all pressure used.

Figure (10) shows the variation of radial position shock speed vs. time for different pressures. The curves decrease as time develops reaching a peak and then slightly increases. As the gas pressure increases the curve continue to rise but still has negative values of speed. Neglecting the negative sign, the radial position shock speed peak is $(41.8\ cm/\mu s)$ for pressure $(4.5\ Torr)$ just before the radial shock hits the axis at $(21.5\ ns)$ after starting of radial phase (Fig. 7). At a pressure $(8.3\ Torr)$ the radial shock speed peak is $(29.9\ cm/\mu s)$ before the radial shock hits the axis at $(29.5\ ns)$ after starting of radial phase.

Figure (11) shows the variation of radial piston (current sheath) speed versus time for different gas pressures. The radial piston speed increases in negative sign reaching to peak and then sharply decreases. As the pressure increases the radial speed piston takes longer time to reach the peak.

Figure (12) shows the variation of pinch elongation speed versus time for different gas pressures. The pinch elongation speed increases exponentially to a value there is constant speed and then increases at fixed time to a higher speed value. However, at low pressure the pinch elongation speed has higher values than as the pressure increased.

Figure (13) displays the variation of I_{pinch} versus pressure. As pressure increases I_{pinch} is rapidly increased reaching to peak at nearly $(4.5\ Torr)$ and then decreased. Obviously, the increased and decreased of I_{pinch} determines the way that neutron yield behave.

Figure (14) shows the computing the neutron yield Y_n as a function of pressure. The pressures had been chosen in order to demonstrate the way the neutron yield varies with pressure. It is clear that Y_n increases rapidly from $(1.5\ Torr)$ to the peak at nearly $(4.5\ Torr)$. Then, the neutron yield also decreases rapidly as the pressure increased. It is obvious that the optimum pressure (for Y_n) is between $(4.5\ Torr)$ and $(5.3\ Torr)$. We note that computed neutron yield versus pressure curve agrees reasonably with the published curve [11]. Also we note that axial speed has an optimum value for deuterium operation. The average axial speed for optimum neutron yield appears to be just below $(6\ cm/\mu s)$ corresponding to a peak axial speed of $(9-10\ cm/\mu s)$ (Fig. 4) and a peak radial speed of some $(25\ cm/\mu s)$ as the plasma focus radial shock goes on axis (Fig. 10).

Conclusion

We studied the computed results, including total current, tube voltage, pinch current, radial and axial trajectories, radial and axial speeds, plasma temperature, and neutron yield. Obviously, the axial position, temperature and voltage tube all continue to rise as pressure lowers to rise. However, radial inward, reflected, and piston positions shifted left hand side due to short duration of radial phase as pressure decreased. Speeds (axial, radial shock and radial piston) increase as pressure is decreased. The code is used to compute the neutron yield versus pressure curve of the PF400J. The computed results agree reasonably well with

the published curves. The results indicate that this code, incorporated gives realistic plasma dynamics and realistic neutron yield without the need of any adjustable parameters, needing only to fit the computed current trace to a measured current trace. It is necessary to note that our calculated results give a good agreement with the published experimental results [9, 14].

References

1. Focus Fusion Society, What is Focus Fusion? From (The Plasma Universe Wikipedia-like Encyclopedia).
2. Lee S. and Saw S. H. (2010), A course on plasma focus numerical experiments, the Abdus Salam – International center for theoretical physics, Italy.
3. Lee, S. (2005), Radiative Dense Plasma Focus Model Computation Package, RADPFV5.008. NTU/NIE NSSE Plasma Radiation Source Laboratory, Singapore.
4. Siahpoush V.; Tafreshi M.A.;Sobhanian S. and Khorram, S. (2005), Adaptation of Sing' Lee model to the Filippov type plasma focus geometry , Plasma, Phys. Control. Fusion 47(7):1065.
5. Goudarzi, S.;Amrollahi R.and Moghaddam, R.S. (2008), A model based on lumped parameters for Filipov type plasma focus devices , J. Fusion Energ., 27(3):195-199.
6. Masoud, M.M.;El-Gamal, H.A.;El-Tayeb, H.A.; Hassouba, M.A. and Abd Al-Halim, M.A. (2007), Magnetohydrodynamic simulation for plasma focus devices, Plasma Devices Operations, 15(4): 263.
7. Lee, S. (1991), A sequential plasma focus, IEEE Trans on Plasma Sc, 19 (5):912.
8. Liu, M. H. and Lee, S. (1998), SXR Radiation Modeling for Neon Plasma Focus. Intern Congress on Plasma Phys, Prague.
9. Silva, P.; Soto, L.; Kies, W. and Moreno, (2004),Pinch evidence in a fast and small plasma focus of only tens of jouls" J Plasma Sources Sci. Technol. 13(2): 329.
10. Seng,L.L. (2009) Lee's Radiative Plasma Focus Model -An Improved Implementation with Auto-tuning of Model Parameters, A Master dissertation, National Institute of Education, Nanyang Technological University .
11. Lee, S.; Saw, S. H., L.; Soto, Springham, S. V. and Moo, S. P. (2009), Numerical experiments on plasma focus neutron yield versus pressure compared with laboratory experiments,Plasma Phys. Control. Fusion 51 (7):75006.
12. Lee, S. (1991) , Experiments with the ICTP – UM 3.3kJ plasma fusion facility, spring college on plasma physics, the Abdus Salam – International center for theoretical physics, Italy.
13. Lee, S. (1998), Scaling of the Plasma Focs - Viewpoint from Dynamics ,International Plasma Focus Symposium at Kudowa, Poland,
14. Saw ,S. H. and Lee, S. (2011), Scaling the plasma focus for fusion energy considerations , International. Journal of Energy Research. 35 (2): 81-88 .

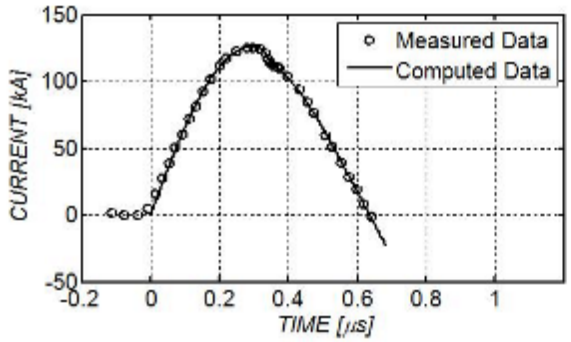

Fig. (1): the variation of tube current vs. time

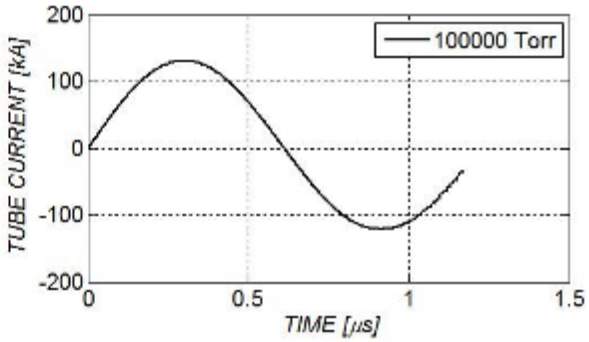

Fig. (2): the variation of tube current vs. time at a high

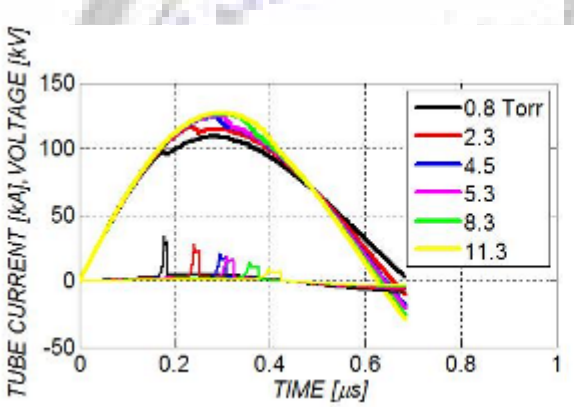

Fig. (3): the variation of tube current (bold curves), and voltage (thin curves) vs. time for different gas pressures

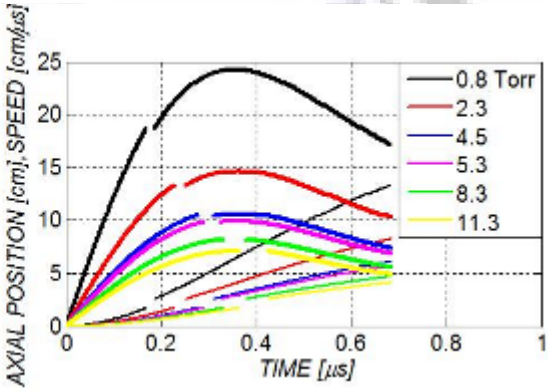

Fig. (4): the variation of axial position (thin curves), and speed (bold curves) vs. time for different gas pressures

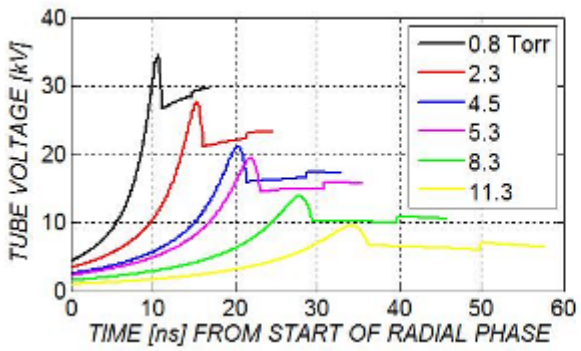

Fig. (5): the variation of tube voltage vs. time for different gas pressures

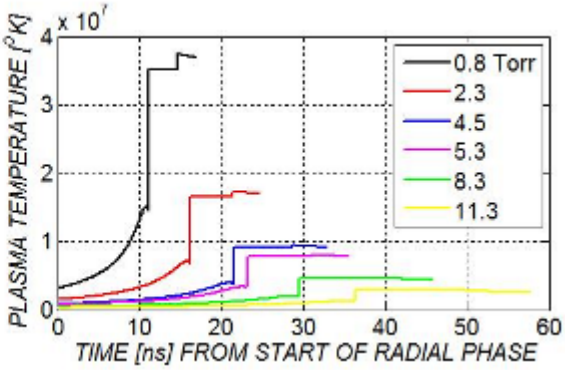

Fig. (6): the variation of plasma temperature vs. time for different gas pressures

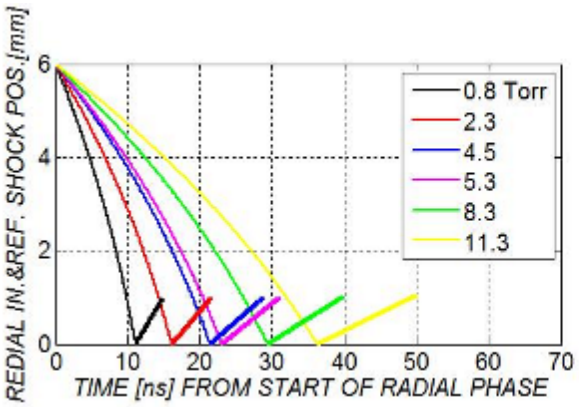

Fig. (7): the variation of inward and reflected shock positions vs. time for different gas pressures

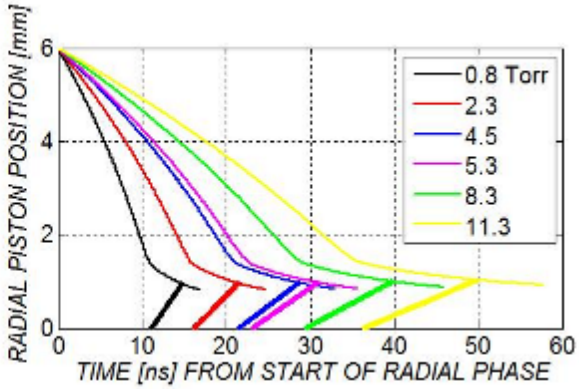

Fig. (8): the variation of radial and reflected shock positions vs. time for different gas pressures

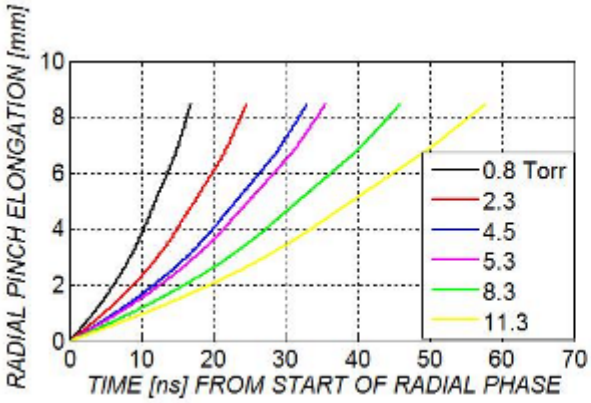

Fig.(9): the variation of radial pinch elongation speed vs. time for different gas pressures

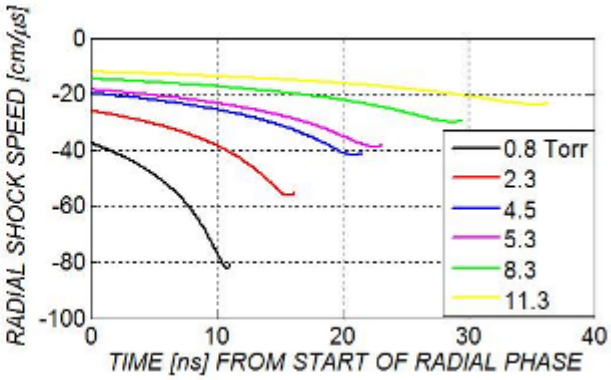

Fig. (10): the variation of radial position shock speed vs. time for different gas pressures

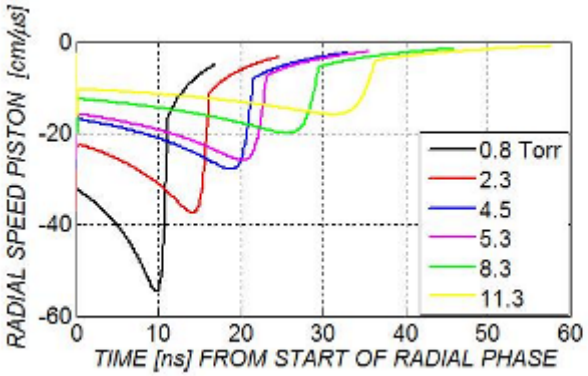

Fig.(11): the variation of radial piston speed vs. time for different gas pressures

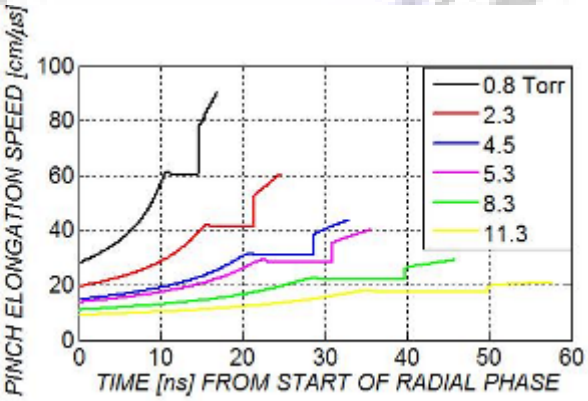

Fig. (12): the variation of pinch elongation speed vs. time for different gas pressures

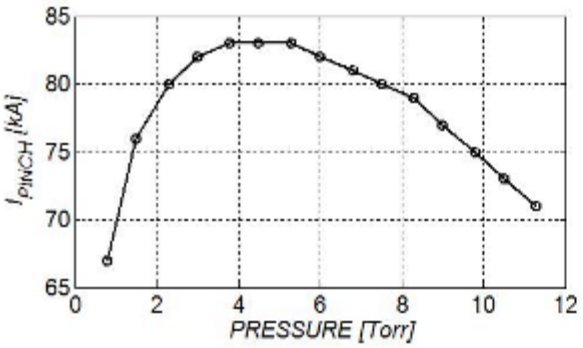

Fig. (13): I_{pinch} vs. gas pressure

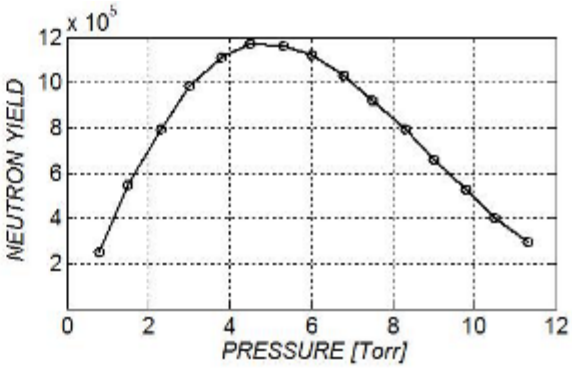

Fig. (14): Y_n vs. gas pressure

دراسة تأثير ضغط الغاز على معلمات ماكنة بؤرة البلازما الكثيفة PF400J

رعد حميد مجيد و مصطفى كامل جاسم و فراس محمود هادي
قسم الفيزياء/كلية التربية -ابن الهيثم/جامعة بغداد
استلم البحث في 19 شباط 2012 قبل البحث في 17حزيران 2012

الخلاصة

انجزت دراسة نظرية لحساب عوامل ميزات بؤرة البلازما الكثيفة عند ضغوط مختلفة لغاز الديوتريوم لماكنة بؤرة البلازما الكثيفة PF400J باستعمال برنامج حسابي عالمي. وتم حساب السرع المحورية والشعاعية ، وفولتية الانبوب ، ودرجات حرارة بلازما ، ونواتج النيوترون عند ضغوط مختلفة من غاز الديوتريوم. حيث تم تقدير اقصى ناتج كلي للنيوترونات ذا مرتبة تتراوح ما بين (10^5) الى (10^6) نيوترون لكل تشغيل عند الضغوط المستعملة. النتائج المحسوبة نظريا تتوافق جيدا مع النتائج العملية المنشورة عالميا.

الكلمات المفتاحية: بؤرة البلازما ، الحاصل النيتروني ، غاز الديتريوم ، برنامج لـي